The significance of calcium ions on *Pseudomonas fluorescens* biofilms – a structural, and mechanical study

Ashkan Safari[§], Olivier Habimana[§], Ashley Allen, Eoin Casey[*]

School of Chemical and Bioprocess Engineering, University College Dublin (UCD), Belfield, Dublin 4, Ireland

[*]Corresponding author. Email: eoin.casey@ucd.ie ; Phone: +353 1 716 1974.

[§]Both authors contributed equally to this work.

Text: 5956 words

References (do not include in the total): 1177

Figures: 197

Tables: 166

TOTAL (excluding references): 6319

Acknowledgments

This work was supported by the European Research Council (ERC), under grant number 278530. The authors thank Dr. Ellen L. Lagendijk from the Institute of Biology Leiden, Netherlands for the gift of the *Pseudomonas fluorescens* PCL1701 strain

Abstract

The purpose of this study was to investigate the effects of calcium ions on the structural and mechanical properties of *Pseudomonas fluorescens* biofilms grown for 48 hours. Advanced investigative techniques such as laser scanning microscopy and atomic force spectroscopy were employed to characterize biofilm structure as well as biofilm mechanical properties following growth at different calcium concentrations. The presence of calcium during biofilm development led to higher surface coverage with distinct structural phenotypes in the form of a granular and heterogeneous surface, compared to the smoother and homogenous biofilm surface in the absence of calcium. The presence of calcium also increased the adhesive nature of the biofilm, while reducing its elastic properties. These results suggests that calcium ions could have a functional role in the biofilm's development and has practical implications in, for example, analysis of biofouling in membrane-based water treatment processes such as nanofiltration or reverse osmosis where elevated calcium concentrations may occur at the solid-liquid interface.

Keywords: *Pseudomonas fluorescens, biofilm,* $CaCl_2$*, force spectroscopy, Young's modulus*

1. Introduction

Biofilms comprise a community of microorganisms attached to a surface, embedded in a matrix of extracellular polymeric substances (EPS), a mixture of macromolecules such as polysaccharides, proteins, nucleic acids, phospholipids and other polymeric compounds which intersperse the cells and mediate adhesion to surfaces (Wingender et al. 1999). The physical stability of the polymer network within the biofilm is enhanced by crosslinking in the EPS matrix, forming a temporary gel (Allison et al. 2000). The concentration of ions, such as calcium, is generally accepted as playing an important role in determining the mechanical properties of biofilms (Ahimou et al. 2007; Korstgens et al. 2001). Studies have demonstrated that the crosslinking of EPS alginate molecules by calcium ions was found to increase the elastic properties of *P.* aeruginosa biofilms (Korstgens et al. 2001), as well as biofilm thickness (Sarkisova et al. 2005). The presence of elevated levels of ions is particularly relevant to pressure-driven membrane processes such as nanofiltration and reverse osmosis which are designed to retain salts and under normal operation create a concentration polarisation (CP) layer of elevated salt concentration adjacent to the membrane-water interface. In these systems biofouling is a well- documented performance limiting problem. Because CP occurs in the same location as biofilm formation, it can be expected that biofilm development occurs in a micro-environment of elevated salt concentration. The presence of such elevated levels of ions is therefore particularly relevant to such processes, which are designed to retain salts. Of these salts, calcium was shown to be the principal element in fouling layers from surface water, as demonstrated in an earlier study(Baker et al. 1995). This unfortunately can lead to inorganic fouling due to scale formation of sparingly soluble inorganic salts, which occurs whenever the ionic salt concentration stream exceeds the equilibrium solubility. Since inorganic scaling and biofouling do not occur in isolation during nanofiltration processes, investigating how one factor impacts the other is therefore crucial for better understanding the membrane fouling. The present study sought to study the effect of different concentrations of a relevant divalent ion, in this case

59 calcium, on the structural and mechanical properties of a *Pseudomonas fluorescens* biofilm model.
60 There is currently a poor understanding of the effect of microenvironments, such as solution
61 composition and shear forces, on biofilm material properties. AFM-based force spectroscopy has
62 emerged as a promising technique allowing the quantification of biofilm adhesive and cohesive
63 forces, however, this has predominantly been applied for single cell adhesion studies, in which
64 this technique was used to characterise the bacterial outer membrane molecules.

65 Nanoindentation experiments have been used to estimate the elastic modulus of the
66 single bacterial cells using the Hertz model (Chen et al. 2012; Francius et al. 2008; Touhami et
67 al. 2003). The Hertzian model is a well-accepted contact mechanics model which consists of
68 indentation into a material to estimate the elastic modulus based on a non-adhesive contact area
69 during indentation (Hertz 1881). Although experimentally challenging, AFM-based,
70 nanoindentation can also be used to estimate the elastic modulus of bacterial biofilm aggregates
71 (Abe et al. 2011; Mosier et al. 2012). More specifically, the viscoelastic properties of biofilms
72 grown on the microbead of an AFM cantilever was directly measured during their compression
73 by a stiff surface via indentation-time (creep) curves, in which the Hertz model was incorporated
74 into a three-element Voigt Standard Linear Solid model (Lau et al. 2009).

75 The retraction part of an AFM force curve can also be used to assess the adhesion
76 properties of biofilms. Different studies were able to demonstrate that increased biofilm
77 adhesive properties is directly linked to the amount of the EPS synthesized during biofilm
78 development (Auerbach et al. 2000; Fang et al. 2000; Oh et al. 2007; Tsoligkas et al. 2012).
79 Although the use of AFM for studying biofilm cohesiveness within biofilms still remains
80 uncommon, its potential use may provide invaluable information concerning the biofilm sample
81 being analysed. In one abrasion study of mixed culture biofilms from activated sludge, AFM was
82 successfully implemented to describe the increasing cohesiveness of the sample with increasing
83 sample depth under elevated shear loading (Ahimou et al. 2007). Since the cohesive and adhesive
84 properties of cells are of critical importance in the factors that dictate biofilm detachment,

85 understanding the functional role of calcium ions in this process would help better understand
86 how biofilms form and proliferate in shear environments.

87 The objective of this study was to investigate the effects of $CaCl_2$ on the mechanical and
88 structural properties of *Pseudomonas fluorescens* biofilms, with particular reference to the
89 measurement of the adhesive and elastic properties at the surface of the different biofilm
90 samples using AFM-based force spectroscopy. These measurements were complemented by
91 CLSM and SEM imaging techniques.

92 2. Materials and Methods

93 2.1 Bacteria Strain and Culture Condition

94 The selected bacterial strain for this study was a mCherry-expressing *Pseudomonas*
95 *fluorescens* PCL1701 (Lagendijk et al. 2010), stored at -80°C in King B broth(King et al. 1954)
96 supplemented with 20% glycerol. Cultures were obtained by inoculating 100 mL King B broth
97 supplemented with gentamicin at a final concentration of 10 μg mL^{-1} using a single colony of a
98 previously grown culture on King B agar (Sigma Aldrich, Ireland) at 28°C. The inoculated
99 medium was then incubated at 28°C with shaking at 75 rpm and left to grow to late exponential
100 growth stages, corresponding to an Optical Densities (OD_{600}) of about 1.0.

101 2.2 Biofilm Growth under Different $CaCl_2$ Concentrations

102 A 5 μL volume of an overnight culture was used to inoculate sterile individual centrifuge
103 tubes (Falcon, Fischer scientific, Ireland) each containing 3 ml King B broth supplemented with
104 gentamicin at a final concentration of 10 μg mL^{-1}. The pH of the King B medium prior
105 inoculation was pH 6.8, which later increased to pH 7.4 following overnight planktonic growth
106 by *Pseudomonas fluorescens*.

107 Two tubes were supplemented with $CaCl_2$ each at final concentrations of 1.5 mM and 15
108 mM. Single autoclaved cover slip disks of 24 mm diameter (Thermo Scientific, Germany), were

109 partially submerged into individual tubes, before sealing each tube with sterile cotton wool.
110 Tubes were then incubated for 48 hours at 28 ºC with shaking at 75 rpm. A schematic of the set-
111 up and a typical biofilm grown at air-liquid line at 1.5 mM $CaCl_2$ (prior to rinsing) are shown in
112 Figure 1S, in the supplementary information section.
113

114 **2.3 Confocal Laser Scanning Microscopy**

115 Following biofilm growth, coverslips were first rinsed in sterile 0.1M NaCl solution by
116 gently dipping the coverslip containing biofilm in a tube containing sterile 0.1M NaCl solution.
117 The coverslip was then carefully placed in a single-well Nunc® Lab-Tek® II Chamber Slide™
118 (VWR, Ireland) filled with sterile phosphate buffered saline solution.
119 Horizontal plane images of the biofilms were acquired using an Olympus FV1000 confocal laser
120 scanning microscope (CLSM) at the Live Cell Imaging core technology facility platform, Conway
121 Institute, UCD. CLSM experiments were repeated twice for each biofilm growth conditions
122 using two independent inoculums. At least 4 to 6 random areas were acquired for each biofilm
123 grown on the air-liquid interface area per coupon per experiment. The excitation wavelength
124 used for mCherry was 559 nm, and emitted fluorescence was recorded within the range of 570 to
125 670 nm. Images were collected through an Olympus UPL SAPO 10x/0.40 air objective with a z-
126 step of 1 µm. 3D projections were performed with Zeiss ZEN imaging software. The structural
127 quantification of biofilms (biovolume, surface coverage, thickness and roughness) was
128 performed using the PHLIP Matlab program developed by J. Xavier (http:
129 //phlip.sourceforge.net/phlip-ml). Biofilm surface volume ratio was obtained from parameters
130 provided by the PHLIP analysis.
131 One-way analysis of variance was performed using MINITAB v15.1 (Minitab Inc., State
132 College, PA, USA) in order to test the significant differences in biovolume quantities (μm^3),
133 surface coverage (%) mean thickness (µm), biofilm roughness, and surface to volume ratio of *P.*

134 *fluorescens* biofilms grown in the presence or absence of $CaCl_2$ with Tukey's test for pair wise
135 comparisons. All tests were performed at 5% significance level.
136

137 **2.4 Scanning Electron Microscopy**

138 Following incubation biofilms were prepared for scanning electron microscopy (SEM)
139 observations. Biofilms were first rinsed by gently dipping the coverslip containing biofilm
140 growth in a tube containing sterile 0.1M NaCl solution. Biofilms were then chemically fixated by
141 submerging coverslips into individual small Petri dishes, each containing 5mL solution
142 containing 2.5% glutaraldehyde (Sigma, Ireland), 0.1 M sodium cacodylate (Sigma, Ireland) and
143 0.075 % (w/v) Ruthenium red (Sigma, Ireland), for 24 hours. All samples were rinsed in sterile
144 MilliQ, followed by a stepwise dehydration treatment by exposing fixated samples to increased
145 ethanol-volumes of 10%, 25%, 50%, 75%, 90% and 100%, each at 10 min intervals. Samples
146 were then exposed to 50% then 100% hexamethyldisilizane (Sigma, Ireland) before drying in air,
147 before gold sputtering using an Eintech K575K coater for 30s at 30 mA. High magnification
148 imaging of biofilms grown at different $CaCl_2$ concentration environments was performed using a
149 Hitachi Quanta 3D FEG scanning electron microscope of the UCD Nano-imaging and Materials
150 Analysis Centre (NIMAC).
151

152 **2.5 AFM-based Force Spectroscopy**

153 The elastic and adhesive properties of *P. fluorescens* biofilms were characterised by analysing
154 indentation and retraction curves obtained from AFM-based Force Spectroscopy measurements.
155 Force measurements were performed using a JPK NanoWizard II BioAFM (JPK Instruments,
156 Germany) integrated with an inverted optical microscope (Nikon, Japan) and a Hamamatsu CCD
157 camera. This ensemble was enclosed in an acoustic isolation chamber, and placed on a vibration
158 isolation table (TS-150, JRS Scientific Instruments, Switzerland). A commercial silicone v-shaped

159 cantilever with a spherical borosilicate tip of 10 μm radius (PT-GS, Novascan Technologies Inc.)
160 was used in this study. The spring constant of the cantilevers was calibrated as 0.12 N/m at the
161 room temperature, using the thermal noise method (Hutter & Bechhoefer 1993). After each
162 force map measurement, several single force curves were recorded on a clean glass in order to
163 observe the possible residual forces on the retraction curves, indicative of the tip contamination.
164 When contaminated, the cantilever was carefully rinsed with ethanol and Milli-Q water, before
165 UV Ozone cleaning (ProCleaner, Bioforce Nanosciences, USA).

166 Prior to measurements, biofilms were first rinsed in sterile 0.1 M NaCl solution, as
167 previously described. Samples were then mounted at the bottom of a JPK liquid cell holder and
168 measurements were carried out on samples submerged in 0.1M NaCl solution (cf. supplementary
169 Figure S2 description of inverted bright field microscopic images of the approached AFM
170 cantilever over the biofilm patch areas). For each biofilm growth condition, force spectroscopy
171 measurements were performed on duplicate biofilms samples grown on separate cover glass
172 slides. Prior to acquisitions, an interval of 30 min was allowed to minimise the thermal noise,
173 causing fluctuations is the recorded signal. Force maps were recorded at various locations on the
174 biofilm samples in a 2-dimensional array of 4 x 4 (16 force curves) over a 10 x 10 μm^2 area. All
175 force spectroscopy experiments were performed in duplicates for each biofilm growth condition,
176 using two independently grown inoculum cultures. Three force maps were obtained for each
177 tested biofilm sample, amounting to a total of 192 force curves for each tested biofilm type. It
178 should be noted that the AFM data in this study was restricted to the biofilm-liquid interface.
179 Force curves were collected at a slow rate of 1 μm/s to minimise the hydrodynamic effects and
180 indentation was made up to a force set-point limit of 9-11 nN.

181 JPK IP data processing software (version 3.3, JPK Instruments) was used for raw data
182 processing and Hertz model fitting based on the protocols explained in user manual (JPK
183 Instrument, 2009). Data processing steps involved converting recorded raw photodetector signal

184 (in Voltage) into the force (in nN), calculating indentation depth, and manually determining the
185 contact point for Hertz model fitting. It is noted that indentation into a deformable sample is
186 obtained by subtracting the Piezo displacement on a rigid mica or glass surfaces (which is only
187 caused by cantilever deflection) from the total Piezo displacement (which is the sum of cantilever
188 deflection and indentation depth) as described for a bacterial cell nanoindentation (Touhami et
189 al. 2003). The elastic modulus was calculated based on the assumption that biofilm is an
190 incompressible material having a constant Poisson's ratio value of 0.5. This is an acceptable
191 assumption as the biofilm is mainly composed of water (95%) (Characklis & Marshall 1990). In
192 previous biofilm studies, a constant Poisson's ratio value within the range of 0.4-0.5 was used
193 (Laspidou & Aravas 2007; Taherzadeh et al. 2010). It is important to note that in a viscoelastic
194 polymeric material the Poisson's ratio typically changes in a time dependent manner from 0.33 in
195 the glassy regime to approximately 0.5 in the rubbery regime due to the flowing properties
196 (Greaves et al. 2011). This may also be expected in biofilms, however it is a largely neglected
197 concept in biofilm mechanics.

198 In the AFM-based nanoindentation testing, determining the contact point is generally the
199 most critical step for fitting the Hertz model into a force-indentation (FI) curve. Defining the
200 contact point has still not been well described in the literature for AFM measurements on
201 biofilms; however it has been widely discussed in studies on individual bacterial cell surfaces
202 (Gaboriaud & Dufrene 2007). It was reported that the initial nonlinear region on the FI curve
203 was potentially affected by both the repulsive surface forces as well as sample surface
204 deformation (Oh et al. 2007). As for the indentation testing of single bacterial cells, contact
205 points are typically chosen at the point at which the force increases from the zero value, which
206 unfortunately do not take into account the initial surface repulsive forces considered to be
207 insufficient to deflect the cantilever (Amoldi et al. 1998). It was only recently that the Hertz
208 model was successfully applied to multilayer inhomogeneous biological samples such as living

209 cells (Kasas et al. 2013; Radotic et al. 2012). This adds weight to the applicability of using the
210 Hertz model in segmented layers of the material. In this study it was necessary to use a multiple
211 layer Hertz fitting approach for the characterisation and analysis of biofilms grown at different
212 $CaCl_2$ concentrations.

213

214 **2.5.1 Probability distribution analysis**

215 Probability density analysis describes the relative likelihoods and distributions of
216 outcomes, defined by the integral of the variable's density over a particular measured range via
217 the area under the density distribution. By using a statistical package provided by Matlab (version
218 R2011a) a lognormal distribution function was found to be the best fit for the data acquired in
219 this study (cf. supplementary section 2.2). The lognormal probability density function has been
220 previously used to describe the distribution of AFM adhesion data for the bacterial cell surfaces
221 (Abu-Lail & Camesano 2003; Eskhan & Abu-Lail 2014; Gordesli & Abu-Lail 2012; Park et al.
222 2009).

223

224 **3. Results and Discussion**

225 **3.1 Biofilm structural and morphological properties**

226 To characterise the effects of $CaCl_2$ on biofilm morphological and structural properties,
227 *Pseudomonas fluorescens* biofilms were grown for two days at the air-liquid interface before being
228 monitored and quantified following CLSM and SEM. Although all biofilms formed a distinct
229 boundary at the air-liquid interface regardless of the presence of $CaCl_2$, the size of this boundary
230 was correlated with the concentration of $CaCl_2$ used during biofilm development (results not
231 shown). Microscopy further revealed differences between the biofilms grown at different
232 concentrations. Figure 1 depicts representative reconstructed 3D projections of *P. fluorescens*
233 biofilms grown at 0mM $CaCl_2$ (Figure 1A), 1.5mM $CaCl_2$ (Figure 1C) and 15mM $CaCl_2$ (Figure

234 1E). Biofilm grown in the absence of $CaCl_2$ had a smoother textured surface (Figure 1A)
235 compared to biofilms grown in the presence of $CaCl_2$ (Figure 1C & E), which showed signs of a
236 rougher surfaces. High magnification images obtained from SEM further corroborated CLSM
237 images revealing that biofilms grown in the absence of $CaCl_2$ were made up of a smooth EPS-
238 like material covering the cells (Figure 1B), whereas a granular-type of EPS could be observed
239 for biofilms grown at 1.5mM (Figure 1D) and 15mM $CaCl_2$ (Figure 1F). Moreover, the granular-
240 type EPS material was found to be located between the cells within biofilms, and was found to
241 be more abundant in biofilms grown at highest $CaCl_2$ concentrations.

242 Based on the CLSM data, the biofilm structural properties could be described in terms of
243 biovolume, surface coverage, mean thickness, roughness as well as surface to volume ratio (Table
244 1), allowing a quantitative comparison of the biofilms grown at different $CaCl_2$ concentrations.
245 Biofilm growth at 15mM were found to have a significantly higher biovolume compared to
246 biofilms grown in the absence of $CaCl_2$ (p=0.027), with mean values of 8.1x 10^5 μm^3 versus 5.0 x
247 $10^5 \mu m^3$. The presence of $CaCl_2$ led to increased surface coverage (p=0.02) compared to biofilms
248 grown at 0mM $CaCl_2$, regardless of the concentration $CaCl_2$ used during growth. No significant
249 effect was observed by the presence or absence of $CaCl_2$ on biofilm thickness (p=0.526) and
250 roughness (p=0.087) values. This could be explained by the presence of shear and capillary force
251 conditions during growth at the air-liquid boundary which consistently levelled the biofilm
252 thickness regardless of the presence of $CaCl_2$. Although the opposite effect was described in
253 *Pseudomonas aeruginosa* biofilms(Sarkisova et al. 2005), where the increasing $CaCl_2$ concentrations
254 led to higher biofilm thickness; the model used for their biofilm growth involved growing
255 biofilm submerged in medium with continual nutrient renewal in their system. While no
256 differences in thickness was observed in this study, larger biomass sediments were observed at
257 the bottom of tubes with increasing $CaCl_2$ concentrations used at the end of each experiment
258 (results not shown), which could be attributed to sedimentation of detached cells.

259 The surface to volume ratio parameter, an indicator of biofilm porosity, showed a significant
260 $CaCl_2$ effect (p=0.03), whereby increased porosity was observed in the presence of $CaCl_2$.
261 Interestingly, no significant structural differences between biofilms grown at 1.5mM or 15mM
262 $CaCl_2$ were observed, as seen by their total biovolume (p=0.2717), surface coverage (p=0.7726),
263 mean thickness (p=0.5265), biofilm roughness (p=0.9724), and surface to volume ratio
264 (p=0.8242) parameters. This suggests that the even small amounts of additional $CaCl_2$ present
265 during biofilm development are enough to influence the biofilm developmental outcome. Based
266 on results presented in Figure 1 and Table 1, the most significant effect of $CaCl_2$ addition was an
267 increased surface coverage on the substratum, most likely influenced by the induced or facilitated
268 initial adhesion on the interface. Consequently, the high biovolume observed with increasing
269 $CaCl_2$ concentration following two days growth can be explained by higher levels of surface
270 coverage induced by the presence of $CaCl_2$. Another aspect of the CLSM data relates to the
271 surface to volume parameter, which is an indicator of biofilm porosity. The higher biofilm
272 porosity in the presence of elevated $CaCl_2$ is an indicator of the presence of voids within
273 biofilms, which can be a sign of larger amounts of EPS within the biofilms shown in Figure
274 1CDEF. The granular EPS form in biofilms could be attributed by the cross-linking properties
275 of $CaCl_2$, which led to the topographical differences compared to smoother like biofilms grown
276 in the absence of $CaCl_2$. Taking into account the qualitative and quantitative biofilm differences
277 from the presence of $CaCl_2$, it was crucial to determine the mechanical properties of these
278 biofilms in order to further assess the significance of divalent ions such as calcium on biofilm
279 properties.
280 Although primarily focused on biofilm structure, the metabolic changes that take place within
281 *Pseudomonas fluorescens* biofilms grown at different calcium concentrations could also be of
282 relevance, such as shifts in pH or the production of specific metabolites. The shift in pH
283 observed over the course of planktonic growth could have been attributed to an alkaline lipase
284 production typically associated by Pseudomonads (Makhzoum et al. 1993; Mckellar & Cholette

285 1984). Pseudomonads, isolated from soils or plant rhizosphere, are known to produce a variety
286 of secondary metabolites that can directly positively or negatively impact the environment in
287 which these organisms find themselves in. One earlier study in particular, Makhzoum,et al
288 (1995) showed that *P. fluorescens* growth and extracellular lipase production were optimal in
289 simple medium, usually composed of a nitrogen source(Makhzoum et al. 1995). This production
290 of lipase was shown to parallel the growth of the organisms usually during the organism's log
291 phase (Stead 1985). Interestingly Makhzoum et al (1995) demonstrated that the addition of
292 calcium in the growth environment strongly stimulated the production of lipase production by
293 360%(Makhzoum et al. 1995). The significance of lipase production could therefore be of
294 relevance in this study for potential beneficial biotechnological applications of engineered
295 biofilms. However, the need to study environmental factors such as calcium concentration on
296 microenvironments within biofilm matrix would be the first step in carrying out potential future
297 applications. This should include but not be limited to the use of pH sensitive sensor dyes (e.g.
298 Snarf) which would enable to localize and map pH microenvironments within the biofilm matrix.
299

300 **3.2 Biofilm elastic properties**

301 In this study, force-indentation (FI) curves were obtained for biofilms grown in the
302 absence and presence of $CaCl_2$. Representative FI curves are shown in Figure 2 up to a force set-
303 point limit of 9-11 nN. From the results, smaller indentation depths were generally observed for
304 biofilm samples grown in the absence of $CaCl_2$ (0.51±0.14 μm) compared to the larger
305 noticeable indentation depths for biofilms samples grown with calcium (2.1±.0.45 and 2.37±0.5
306 μm for 1.5 mM and 15 mM $CaCl_2$ respectively). Considering biofilms grown without
307 supplemental $CaCl_2$, a much short initial non-linear indentation region may also be identified,
308 despite being characterised as stiff due to a linear FI profile. Biofilm samples grown at two
309 different $CaCl_2$ concentrations showed large nonlinear behaviour at a higher indentation depth
310 which may indicate deformation of a softer surface layer. These explanations are in accordance

311 with microscopic observations of *P. fluorescens* cells and EPS sugar residues shown in Figure S11
312 in the supplementary document where only some parts of the biofilms grown without $CaCl_2$
313 were covered by EPS sugar residues, and the AFM tip was likely in contact with surface cells
314 with a smaller amount of EPS. In contrast, a more homogenous and substantial EPS sugar
315 residue layer covered the biofilm's surface when $CaCl_2$ was present.

316 As shown in Figure 2, different segments of the indentation curve showed a noticeable change
317 prior to and after *transition points*, in which the initial nonlinear behaviour could be distinguished
318 from secondary indentation behaviour. This may indicate the existence of different biofilm sub-
319 layers and suggests that the biofilms are structurally and chemically stratified which has been
320 previously described (Habimana et al. 2009; Stewart & Franklin 2008). It is noted that in this
321 study, the initial nonlinear region was associated with the compressive surface deformation,
322 ignoring the effect of initial surface forces as previously described (Volle et al. 2008a; Volle et al.
323 2008b)

324 In order to use a systematic method to justify the *transition point* and to distinguish between initial
325 and secondary FI profiles, the point of intersection between the fitted Hertzian model and the
326 experimental FI curve was used (see Figures S3a, S4a and S5a). Consequently, individual Hertz
327 models were fitted into these selected segments, providing two distinctive values of elastic
328 modulus (see Figures S3b & c, S4 b & c and S5 b & c). Elastic modulus values and
329 corresponding indentation depths prior to *transition point* are given by *E1* and *D1*, while the
330 elastic modulus and indentation depth after *transition point* are denoted by *E2* and *D2* respectively.
331 The force at the *transition point* was analysed for each experiment individually, determined as
332 1.64±0.48, 1.81±0.37 and 1.88±0.84 nN (Mean±SD) for biofilm samples without calcium, and
333 with 1.5 mM and 15 mM $CaCl_2$ respectively. It should be noted that the indentation depths were
334 fitted within the 10% indentation validity range for the Hertz model based on the total thickness
335 of the biofilm samples provided by CSLM (Table 1). Table 2 summarises *E1* and *E2* values with

336 their corresponding *D1* and *D2* values for all groups (mean data for each repeat is shown in
337 supplementary Figure S6). In summary, an indentation hypothesis based on two decoupled
338 biofilm surface layers has provided explanations for the behaviour shown in Figure 3

339 The larger value of *E1* for the biofilms grown in the absence of $CaCl_2$ (*E1*=2.13 kPa),
340 was probably due to the deformation of a thinner outer layer, which was significantly influenced
341 by a stiffer secondary layer (*E2*=10.1 kPa). However, in the case of biofilms grown in the
342 presence of $CaCl_2$, the lower *E1* value (*E1*=0.25 and 0.23 kPa for 1.5 and 15mM $CaCl_2$
343 respectively) was likely associated with a thicker soft outer layer, which may not be significantly
344 influenced by a less stiff secondary layer (*E2* =2.34 and 1.24 kPa for 1.5 and 15mM $Cacl_2$
345 respectively).

346 As can be seen in Table 2, substantial variations in the elastic modulus for individual
347 samples both within and between the samples. Because of the high variability of the measured
348 data sets, a lognormal probability density function was used to describe the distribution of the
349 data and estimate the most probable (MP) elastic modulus value for each group (cf Figure S7 in
350 supplementary information section).

351 Overall, the higher elastic modulus observed for biofilm samples grown in the absence
352 of $CaCl_2$ could partly be due to the higher number of (rigid) cells and comparatively lower
353 amounts of softer EPS at the surface layers. This is in contrast to biofilms grown with added
354 $CaCl_2$ where higher levels of EPS was present and were covered the surface homogeneously. As
355 previously mentioned, these explanations have been supported by microscopic observations of
356 the cells and EPS (see Figure S 11 in the supplementary document). An increase in the amount
357 of EPS in the presence of elevated calcium concentrations was reported for *P. aeruginosa* biofilms
358 (Sarkisova et al. 2005). Another study also suggested that the overproduction of EPS surface
359 layers of a *mixed culture biofilm* could have been attributed to the adsorption of calcium ion at that

360 biofilm's boundary surface layer, where crosslinks and cells were loosely associated with one
361 another (Ahimou et al. 2007).

362 Biofilms have been previously described as composite materials, consisting of solid
363 biomass including bacterial cells and EPS as well as micro and macro scale pores (Laspidou &
364 Aravas 2007). The approach taken in this present study validates the composite material concept
365 through the use of a *composite elastic modulus,* in which both rigid elastic cells and softer EPS gel
366 can contribute to a single elastic modulus value. The composite elastic modulus is usually
367 described by the general rule of mixtures, expressed in equation 1 (Jones 1999) where E_m and E_d
368 are the elastic modulus of a given matrix and the dispersed materials. In this study the EPS of
369 the biofilm matrix was expressed as E_m, and the dispersed cells within the matrix as E_d . The
370 volume fraction of both EPS and dispersed cells within the matrix were expressed as V_m and V_d
371 respectively. The total volume of the material (i.e. biofilm mixture) is defined as the sum of the
372 volumes of all individual phases. In one earlier study, the elastic modulus of alginate EPS
373 extracted from an *Azotobacter vinelandii* biofilm which was measured at 2-4 kPa (Moresi et al.
374 2004), was found to be within the range reported for biopolymers (1-100 kPa) (Clark &
375 Rossmurphy 1985). In this study, the elastic modulus of bacterial cells was found to be higher
376 than that of biopolymeric substances, ranging between 180 to 6100 kPa based on the Hertz
377 model based nanoindentation studies (Chen et al. 2012; Francius et al. 2008; Touhami et al.
378 2003). As shown in equation 1, the larger V_m with lower E_m could result in the lower elastic
379 modulus of the biofilm as a whole (E).

380 Equation 1

$$E = E_m V_m + E_d V_d$$

381 Considering that AFM experiments are typically performed at the biofilm-liquid
382 interface, the significance of biofilm porosity during nanoindentation cannot be neglected,
383 especially when the biofilm at that region is typically 50% more porous than in the deeper layers
384 of the biofilm (Zhang & Bishop 1994). It is generally accepted that higher porosity can lead to a
385 reduction in material elasticity (Phani & Niyogi 1987). This observation can also be applied to
386 biofilms, as described in earlier studies, in which increases in biofilm stiffness was observed as a
387 direct consequence of blocking pores through compressive deformations (Casey 2007; Laspidou
388 & Aravas 2007). In this study, biofilm porosity analysis based on cell biomass and EPS (Figure S
389 12 and S 13 in the supplementary document) showed no significant difference between the
390 samples grown with and without calcium. Therefore, a reduction in the elastic modulus of
391 biofilms may not necessarily be attributed to the porosity of the biofilm structure. This is also
392 consistent with earlier studies showing a more porous *P. aeruginosa* biofilm structure at higher
393 calcium concentrations (Sarkisova et al. 2005).

394 The mean elastic value of 32.96±22.09 kPa (secondary layer) reported in this study for
395 biofilms grown in the absence of calcium was found to be well within the range of 15-170 kPa,
396 as previously reported for early stage *P. aeruginosa* biofilms (Lau et al. 2009). Moreover, the mean
397 elastic modulus values of 3.57±2.42 and 2.71±1.33 kPa for biofilm grown under 1.5mM and
398 15mM $CaCl_2$ environments respectively was also found to be within the of range of 0.58-2.61
399 kPa, as reported for a more mature, EPS laden *P. aeruginosa* biofilms (Mosier et al. 2012).

400 **3.3 Biofilm adhesive Properties**

401 The adhesive properties of biofilm samples as measured using borosilicate spherical
402 AFM probes was quantified from retraction curve data in terms of adhesive force (F_{adh}) in
403 nanoNewton (nN) and adhesion energy (E_{adh}) in attoJoule (aJ). The adhesive energy, E_{adh}, is
404 measured as the area under the retraction curve as a result of sample stretching from its original
405 contact point line (Figure 4). This energy is related to the force of adhesion, F_{adh}, as shown in

406 equation 2, where h is the separation distance. In this study, adhesion energy was obtained using
407 JPK IP data processing software. In Figure 4, the large hysteresis between approach and
408 retraction curves is due to a significant viscoelastic behaviour observed for the EPS at the sample
409 surface during the loading and unloading cycle.

$$E_{adh} = -\int_{h_1}^{h_2} F\, dh$$

Equation 2

410

411 Typical retraction curves were selected and presented in Figure 5 depicting the
412 adhesiveness of biofilms grown in the presence or absence of calcium. The adhesive properties
413 described by multiple adhesion events are likely to be associated with long-ranged polyprotein
414 stretching and failure events, as previously observed for the surface EPS of *E. coli* biofilms
415 (Tsoligkas et al. 2012). AFM studies performed on adhered single cells demonstrated a wave-like
416 adhesion behaviour due to the stretching and unfolding of polymeric macromolecules found on
417 the cell outer-membrane such as polysaccharides and proteins (Cross et al. 2007; Francius et al.
418 2008). The magnitude of the adhesive forces and area under the retraction curves was found to
419 increase with increasing calcium concentration, which could be associated with larger amounts of
420 EPS produced at the surface of biofilm samples. Again, this was confirmed by microscopic
421 observations showing a substantial amount of EPS sugar residues covering the biofilm's surface
422 in the presence of $CaCl_2$ (see Figure S11 in supplementary document), and similarly described by
423 other researchers (Auerbach et al. 2000; Fang et al. 2000; Oh et al. 2007; Tsoligkas et al. 2012).
424 As shown in Figure 5A, in the case of biofilm grown without calcium, a numbers of retraction
425 curves showed a single adhesion event (green curve), probably due to the contact with the
426 surface of the bacterial cells, also previously reported for early stage *E. coli* biofilms (Tsoligkas et
427 al. 2012). In several other samples lower adhesion forces were observed, which can be explained
428 as the presence of small residual EPS amounts attached to the AFM tip surface (red curve)
429 following indentation procedures. As for the adhesion behaviour of biofilms grown in the

430 presence of calcium ions, pronounced elongated adhesion profiles were observed (Figure 5B),
431 distinctly characterized by a significant number of adhesion events. The magnitude of these
432 events also could also been attributed to a specific highly adhesive EPS type synthesized during
433 biofilm development.

434 The average adhesive force and separation energy following contact with biofilm grown
435 in the presence or absence of calcium ions are summarized in table 3. The average and standard
436 deviation of adhesion data for each replicate as presented in Figure S9 and S10 (cf.
437 Supplementary information section), indicated large variations due to the differences in the
438 amount of EPS and heterogeneity of biopolymer molecules on the surface of biofilm samples, as
439 previously observed on the bacterial cell surface (Camesano & Abu-Lail 2002). As reported in
440 table 3, the most probable value of adhesion force and energy data were estimated by lognormal
441 probability density analysis for each group, showing higher values with increasing calcium (see
442 Figure S11). Recently, the higher adhesive force values was suggested to be associated with
443 stronger polyprotein stretching at the surface EPS of *E. coli* biofilms (Tsoligkas et al. 2012).
444 Furthermore, the increase in adhesion energy was shown to be related to the greater level of EPS
445 attached to the AFM tip surface (Li & Logan 2004). The distribution data for biofilm samples
446 grown in the absence of $CaCl_2$ showed that the majority of measured adhesive forces ranged
447 from nearly zero to greater than 1 nN (see Figure S11a), which was found to fit the range
448 reported for biopolymer molecules at the surface of the bacterial cells (Camesano & Abu-Lail
449 2002) and early stage *E. coli* (Tsoligkas et al. 2012) and *P. aeruginosa* biofilm surfaces (Lau et al.
450 2009). By comparing the elasticity (Figure S6a-c in supplementary) and adhesion data (Figure S9
451 and s10 in supplementary) for each repeat, higher adhesion rates corresponded to lower elastic
452 modulus values, which were generally associated with softer and more sticky biofilm surface
453 layers.

454

455 **CONCLUSION**

456 The aim of this study was to use AFM-based nanomechanical approaches to explain the
457 effect of supplemental calcium in the form of $CaCl_2$ on the properties of *Pseudomonas fluorescens*
458 biofilms. It was shown that the addition of $CaCl_2$ during biofilm growth significantly affected
459 the structural and mechanical properties of the biofilms. From the measured AFM results
460 combined with SEM/CLSM, it was concluded that the addition of $CaCl_2$ increased the amount
461 of EPS. The AFM data showed reduced stiffness, higher viscous effect (larger hysteresis) as well
462 as larger adhesive values at the surface of biofilm with increasing $CaCl_2$ concentration. These
463 trends are consistent with the production of more EPS as the $CaCl_2$ concentration increased. A
464 composite approach was proposed for the analysis of the AFM elasticity data. This study has
465 shed light on the use of AFM-based indentation analysis of a biofilm structure which provides
466 the basis for future studies which should address the cell-to-EPS ratios and a stratified biofilm
467 layer approach.

References

Abe Y, Polyakov P, Skali-Lami S, Francius G. 2011. Elasticity and physico-chemical properties during drinking water biofilm formation. Biofouling.27:739-750.

Abu-Lail NI, Camesano TA. 2003. Role of lipopolysaccharides in the adhesion, retention, and transport of *Escherichia coli* JM109. Environ Sci Technol.37:2173-2183.

Ahimou F, Semmens MJ, Novak PJ, Haugstad G. 2007. Biofilm cohesiveness measurement using a novel atomic force microscopy methodology. Appl Environ Microb.73:2897-2904.

Allison DG, Gilbert P, Lappin-Scott HM, Wilson M. 2000. Community structure and co-operation in biofilms Cambridge, UK ; New York: Society for General Microbiology. Symposium (59th : 2000 : Exeter England),. p. ix, 349 p.

Amoldi M, Kacher CM, Bauerlein E, Radmacher M, Fritz M. 1998. Elastic properties of the cell wall of *Magnetospirillum gryphiswaldense* investigated by atomic force microscopy. Appl Phys a-Mater.66:S613-S617.

Auerbach ID, Sorensen C, Hansma HG, Holden PA. 2000. Physical morphology and surface properties of unsaturated *Pseudomonas putida* biofilms. J Bacteriol.182:3809-3815.

Baker J, Stephenson T, Dard S, Cote P. 1995. Characterization of Fouling of Nanofiltration Membranes Used to Treat Surface Waters. Environ Technol. Oct;16:977-985.

Camesano TA, Abu-Lail NI. 2002. Heterogeneity in bacterial surface polysaccharides, probed on a single-molecule basis. Biomacromolecules.3:661-667.

Casey E. 2007. Tracer measurements reveal experimental evidence of biofilm consolidation. Biotechnol Bioeng.98:913-918.

Characklis WG, Marshall KC. 1990. Biofilms: A Basis for an Interdisciplinary Approach. In: In: WG Characklis and KC Marshall (Eds), Biofilms, Wiley-Interscience. New York: John Wiley & Sons.

Chen Y, Norde W, van der Mei HC, Busscher HJ. 2012. Bacterial Cell Surface Deformation under External Loading. Mbio.3.

Clark AH, Rossmurphy SB. 1985. The Concentration-Dependence of Bio-Polymer Gel Modulus. Brit Polym J.17:164–168.

496 Cross SE, Kreth J, Zhu L, Sullivan R, Shi WY, Qi FX, Gimzewski JK. 2007. Nanomechanical properties of
497 glucans and associated cell-surface adhesion of *Streptococcus mutans* probed by atomic force
498 microscopy under *in situ* conditions. Microbiology-Sgm.153:3124-3132.

499 Eskhan AO, Abu-Lail NI. 2014. A new approach to decoupling of bacterial adhesion energies
500 measured by AFM into specific and nonspecific components. Colloid and polymer science.292:343-
501 353.

502 Fang HHP, Chan KY, Xu LC. 2000. Quantification of bacterial adhesion forces using atomic force
503 microscopy (AFM). Journal of microbiological methods.40:89–97.

504 Francius G, Lebeer S, Alsteens D, Wildling L, Gruber HJ, Hols P, De Keersmaecker S, Vanderleyden J,
505 Dufrene YF. 2008. Detection, localization, and conformational analysis of single polysaccharide
506 molecules on live bacteria. Acs Nano.2:1921–1929.

507 Gaboriaud F, Dufrene YF. 2007. Atomic force microscopy of microbial cells: Application to
508 nanomechanical properties, surface forces and molecular recognition forces. Colloid Surface
509 B.54:10-19.

510 Gordesli FP, Abu-Lail NI. 2012. The role of growth temperature in the adhesion and mechanics of
511 pathogenic *L. monocytogenes*: an AFM study. Langmuir.28:1360–1373.

512 Greaves GN, Greer AL, Lakes RS, Rouxel T. 2011. Poisson's ratio and modern materials. Nat
513 Mater.10:986-986.

514 Habimana O, Meyrand M, Meylheuc T, Kulakauskas S, Briandet R. 2009. Genetic Features of Resident
515 Biofilms Determine Attachment of *Listeria monocytogenes*. Appl Environ Microb.75:7814–7821.

516 Hertz H. 1881. Über die berührung fester elastischer Körper (On the contact of rigid elastic solids). J
517 Reine Angew Mathematik.92:39 – 60.

518 Hutter JL, Bechhoefer J. 1993. Calibration of Atomic-Force Microscope Tips. Rev Sci Instrum.64:1868-
519 1873.

520 Jones RM. 1999. Mechanics Of Composite Materials: Taylor & Francis.

521 Kasas S, Longo G, Dietler G. 2013. Mechanical properties of biological specimens explored by atomic
522 force microscopy. Journal of Physics D: Applied Physics.46:133001.

523 King EO, Ward MK, Raney DE. 1954. 2 Simple Media for the Demonstration of Pyocyanin and
524 Fluorescin. J Lab Clin Med.44:301-307.

525 Korstgens V, Flemming HC, Wingender J, Borchard W. 2001. Influence of calcium ions on the
526 mechanical properties of a model biofilm of mucoid *Pseudomonas aeruginosa*. Water Sci
527 Technol.47:9.

528 Lagendijk EL, Validov S, Lamers GEM, de Weert S, Bloemberg GV. 2010. Genetic tools for tagging
529 Gram-negative bacteria with mCherry for visualization in vitro and in natural habitats, biofilm and
530 pathogenicity studies. Fems Microbiol Lett.305:81-90.

531 Laspidou C, Aravas N. 2007. Variation in the mechanical properties of a porous multi-phase biofilm
532 under compression due to void closure. Water Sci Technol.55:447–453.

533 Lau PCY, Dutcher JR, Beveridge TJ, Lam JS. 2009. Absolute quantitation of bacterial biofilm adhesion
534 and viscoelasticity by microbead force spectroscopy. Biophys J.96:2935-2948.

535 Li X, Logan BE. 2004. Analysis of bacterial adhesion using a gradient force analysis method and
536 colloid probe atomic force microscopy. Langmuir.20:8817-8822.

537 Makhzoum A, Knapp JS, Owusu RK. 1995. Factors Affecting Growth and Extracelluar Lipase
538 Production by Pseudomonas-Fluorescens 2d. Food Microbiol. Aug;12:277-290.

539 Makhzoum A, Owusu RK, Knapp JS. 1993. The Conformational Stability of a Lipase from a
540 Psychrotrophic Pseudomonas-Fluorescens. Food Chem.46:355-359.

541 Mckellar RC, Cholette H. 1984. Synthesis of Extracellular Proteinase by Pseudomonas-Fluorescens
542 under Conditions of Limiting Carbon, Nitrogen, and Phosphate. Applied and Environmental
543 Microbiology.47:1224-1227.

544 Moresi M, Bruno M, Parente E. 2004. Viscoelastic properties of microbial alginate gels by oscillatory
545 dynamic tests. J Food Eng.64:179–186.

546 Mosier AP, Kaloyeros AE, Cady NC. 2012. A novel microfluidic device for the in situ optical and
547 mechanical analysis of bacterial biofilms. Journal of microbiological methods.91:198–204.

548 Oh YJ, Jo W, Yang Y, Park S. 2007. Influence of culture conditions on *Escherichia coli* O157 : H7
549 biofilm formation by atomic force microscopy. Ultramicroscopy.107:869–874.

550 Park BJ, Haines T, Abu-Lail NI. 2009. A correlation between the virulence and the adhesion of *Listeria*
551 *monocytogenes* to silicon nitride: An atomic force microscopy study. Colloid Surface B.73:237–243.

552 Phani KK, Niyogi SK. 1987. Young Modulus of Porous Brittle Solids. J Mater Sci.22:257-263.

553 Radotic K, Roduit C, Simonovic J, Hornitschek P, Fankhauser C, Mutavdzic D, Steinbach G, Dietler G,
554 Kasas S. 2012. Atomic force microscopy stiffness tomography on living Arabidopsis thaliana cells
555 reveals the mechanical properties of surface and deep cell-wall layers during growth. Biophysical
556 journal. Aug 8;103:386-394. Epub 2012/09/06.

557 Sarkisova S, Patrauchan MA, Berglund D, Nivens DE, Franklin MJ. 2005. Calcium-induced virulence
558 factors associated with the extracellular matrix of mucoid *Pseudomonas aeruginosa* biofilms. J
559 Bacteriol.187:4327-4337.

560 Stead D. 1985. Microbial lipases: their characteristics, role in food spoilage and industrial uses. J
561 Dairy Res. 19861030 DCOM- 19861030;53:485-505.

562 Stewart PS, Franklin MJ. 2008. Physiological heterogeneity in biofilms. Nat Rev Microbiol.6:199-210.

563 Taherzadeh D, Picioreanu C Fau - Kuttler U, Kuttler U Fau - Simone A, Simone A Fau - Wall WA, Wall
564 Wa Fau - Horn H, Horn H. 2010. Computational study of the drag and oscillatory movement of
565 biofilm streamers in fast flows. Biotechnol Bioeng. 20091229 DCOM- 20100226;105:600-610.

566 Touhami A, Nysten B, Dufrene YF. 2003. Nanoscale mapping of the elasticity of microbial cells by
567 atomic force microscopy. Langmuir.19:4539-4543.

568 Tsoligkas AN, Bowen J, Winn M, Goss RJM, Overton TW, Simmons MJH. 2012. Characterisation of
569 spin coated engineered *Escherichia coli* biofilms using atomic force microscopy. Colloid Surface
570 B.89:152-160.

571 Volle CB, Ferguson MA, Aidala KE, Spain EM, Nunez ME. 2008a. Quantitative changes in the elasticity
572 and adhesive properties of *Escherichia coli* ZK1056 prey cells during predation by *bdellovibrio*
573 *bacteriovorus* 109J. Langmuir. Aug 5;24:8102-8110.

574 Volle CB, Ferguson MA, Aidala KE, Spain EM, Nunez ME. 2008b. Spring constants and adhesive
575 properties of native bacterial biofilm cells measured by atomic force microscopy. Colloid Surface B.
576 Nov 15;67:32-40.

577 Wingender J, Neu TR, Flemming H-C. 1999. Microbial extracellular polymeric substances :
578 characterization, structure, and function. Berlin ; New York: Springer. p. xiv, 258 p.

579 Zhang TC, Bishop PL. 1994. Density, Porosity, and Pore Structure of Biofilms. Water Res.
580 Nov;28:2267–2277.

581

582

583

584 **Table 1**: Different parameters of biofilm formed by *Pseudomonas fluorescens* strain PCL 1701 in the

585 absence and presence of 1.5mM or 15mM $CaCl_2$ as studied by Confocal Laser Scanning

586 Microscopy and analysed with PHLIP and ImageJ. Values represent mean of 6 biofilm areas.

587 Error bars depict standard error of the mean.

588

589

	Total biovolume [µm3]	Substratum coverage [%]	Mean thickness [µm]	Biofilm roughness	Surface/volume ratio
0mM $CaCl_2$	508587 ± 23265	29.3 ± 1.6	43.1 ± 4.0	0.49 ± 0.004	1.24 ± 0.16
1.5mM $CaCl_2$	701374 ± 72703	45.7 ± 5.0	44.4 ± 5.2	0.45 ± 0.017	1.19 ± 0.17
15mM $CaCl_2$	818390 ± 49900	47.8 ± 1.9	33.3 ± 1.5	0.46 ± 0.016	1.04 ± 0.31

590
591

592 **Table 2** Mean and most probable elastic modulus (E) values for all biofilm groups as well as

593 their indentatiuon depths (D)

594

595

Sample	*D1* (μm)	*E1* (kPa)		*D2* (μm)	*E2* (kPa)	
	Mean±SD	**Mean±SD**	**MP**	**Mean±SD**	**Mean±SD**	**MP**
0mM	0.27±0.1	6.23±3.24	2.13	0.25±0.087	32.96±22.09	10.1
1.5mM	1.21±0.03	0.38±0.21	0.25	0.9±0.29	3.57±2.42	2.34
15mM	1.27±0.33	0.39±0.24	0.23	1.1±0.31	2.71±1.33	1.24

596 * MP is the most probable value estiamted by probability density disticution analysis

597

Table 3 Mean and most probable adheion data values for all biofilm groups

Sample	Adhesive force (nN)		Work of adhesion (aJ)	
	Mean±SD	**MP**	**Mean±SD**	**MP**
0mM	0.61±0.56	0.085	1106.31±1815.74	43.13
1.5mM	1.03±0.64	0.48	2678.80±1791.78	1198.53
15mM	2.06±1.03	1.38	5173.64±3442.80	2602.39

Figures

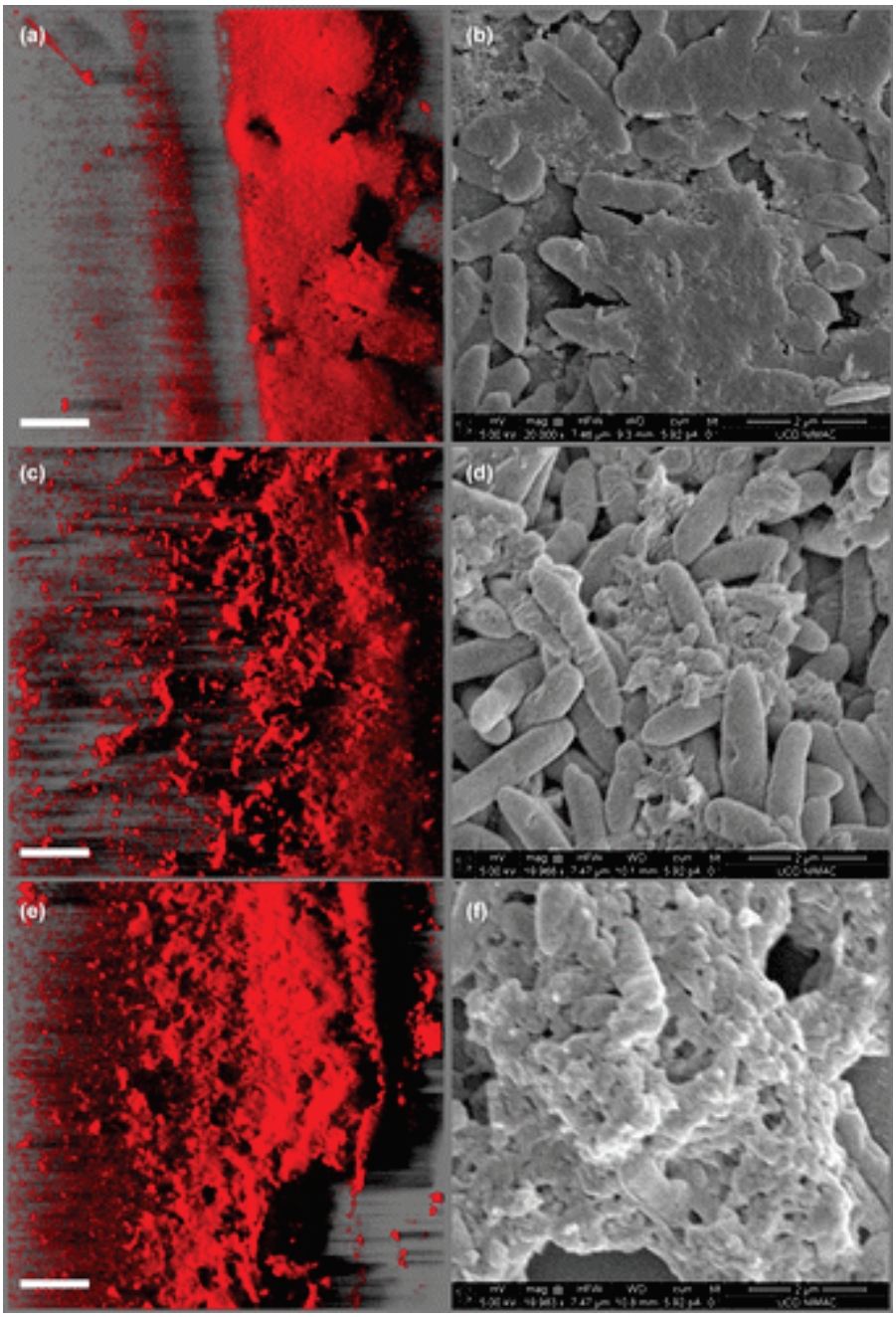

Figure 1: Representative *P. fluorescens* PCL1701 two-day old biofilms grown at different $CaCl_2$ concentrations. Side view 3D projections were aquired from CLSM image of following growth at 0mM (A) , 1.5mM (C) and 15mM (E) $CaCl_2$. Thick white scale bar on projected images represent 200 µm. Corresponding SEM images depict *P. fluorescens* bioflms grown at 0mM (B), 1.5mM (D) and 15mM (F) $CaCl_2$. Thin scale bar on SEM images represent 2 µm.

617

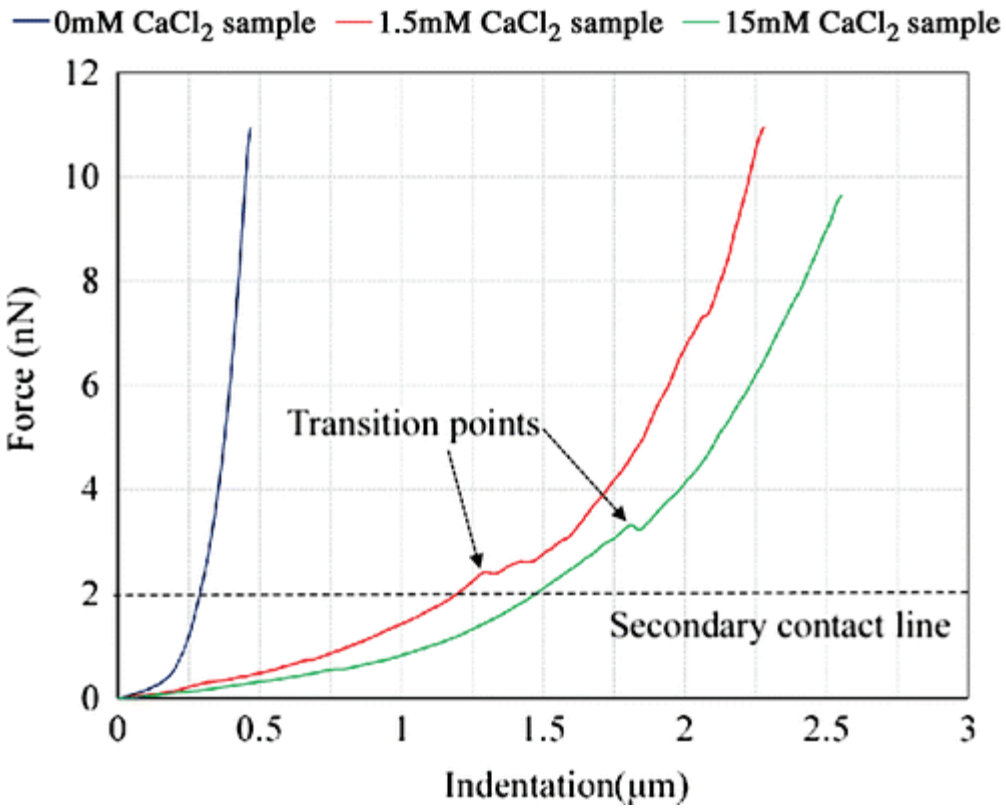

618

619

620 **Figure 2** Elasticity profiles of biofilms in the form of representative measured force-indentation

621 data following growth at 0mM (blue), 1.5mM (red) and 15mM (green) $CaCl_2$,

622

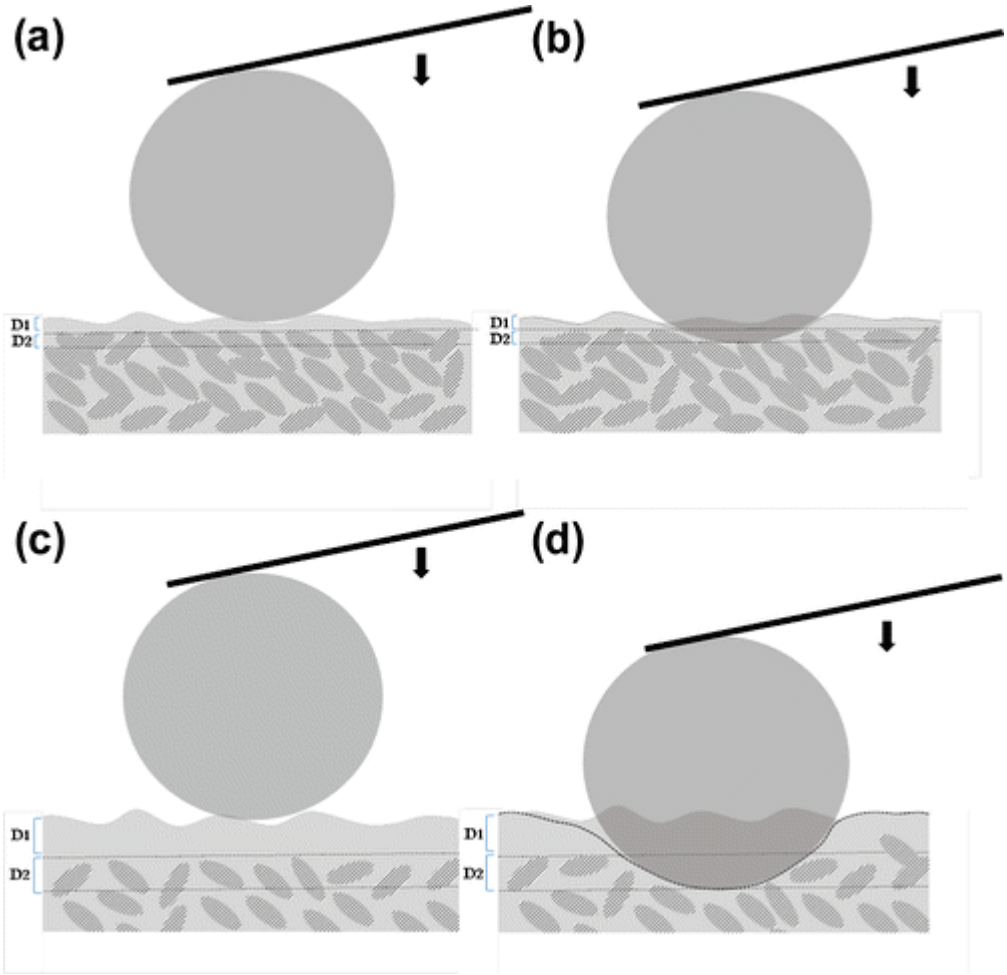

Figure 3 Schematics of proposed indentation behaviour for localised decoupled layers deformation: biofilm without calcium at contact point (a) and at final indentation depth (b); biofilm with added calcium at contact point (c) and at final indentation depth (d);

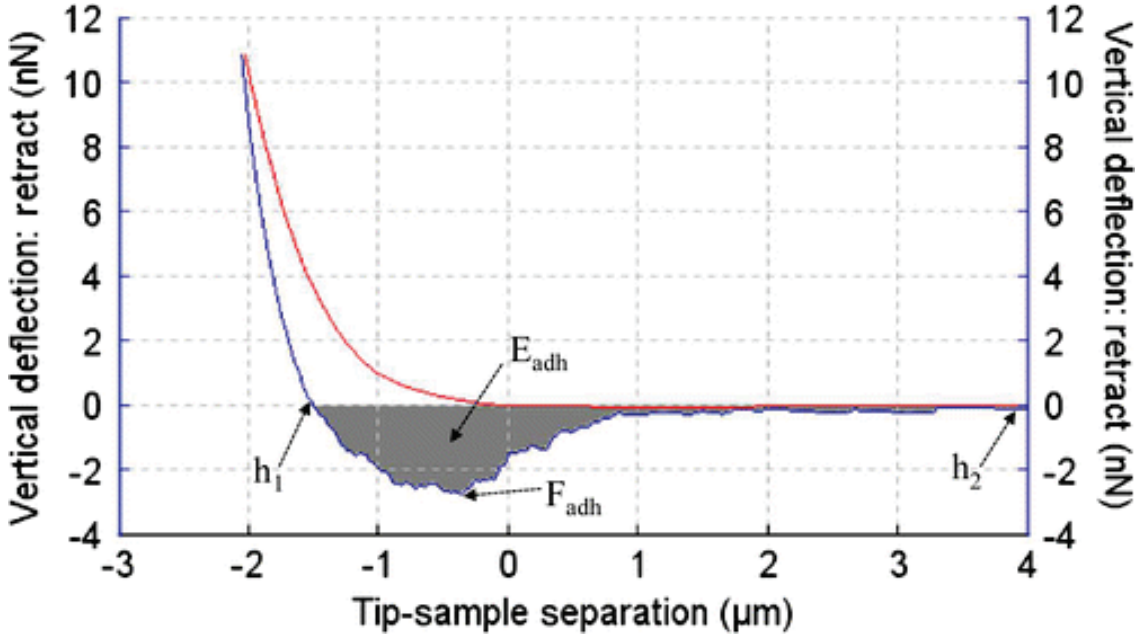

Figure 4: A typical FI curve measured for biofilms with CaCl2 15 mM (b), showing appraoch (red), and retraction (blue) curves, as well as grey area of adhesion energy under the retraction curve

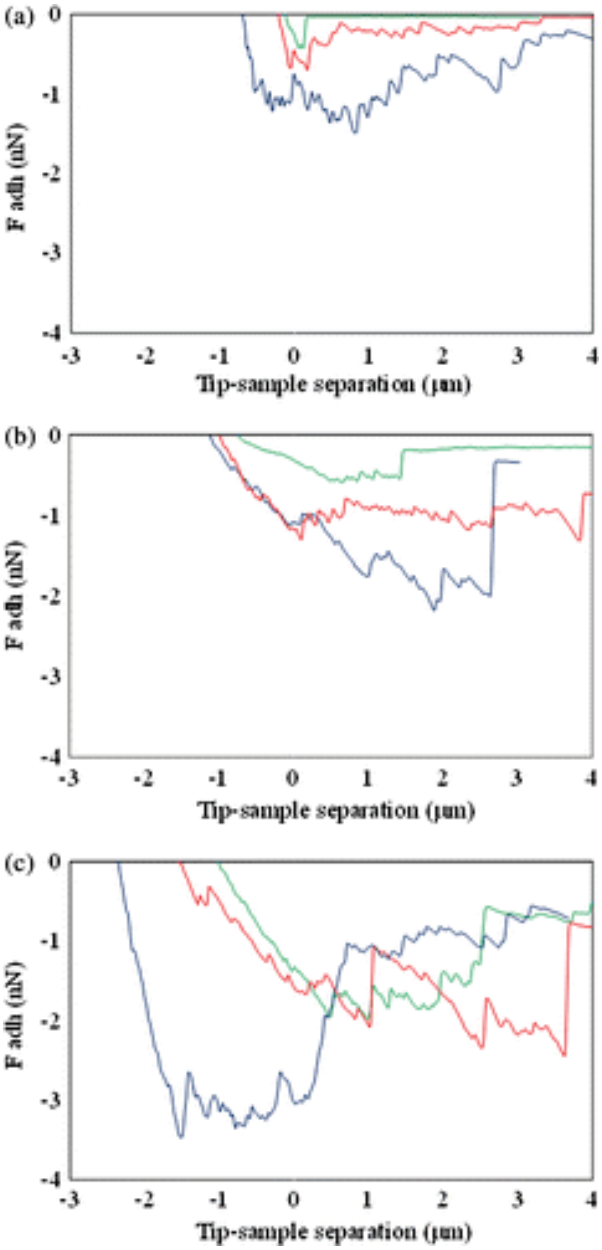

Figure 5 Multiple adhesion events are shown for several typical biofilm without calcium (a), and with $CaCl_2$ at the concentrations of 1.5 mM (b) and 15 mM (c)